A CRITICAL PARAMETRIC INVESTIGATION OF A SOLAR DISH CONCENTRATOR INTEGRATED WITH A STIRLING POWER ENGINE

Dimitrios N. KORRES[1], Christos SAMMOUTOS[1], Panagiotis LYKAS[1], Saša R. PAVLOVIC[2], Marko PERIC[2], Christos TZIVANIDIS[1,*], Evangelos BELLOS[3]

[1] Department of Thermal Engineering, School of Mechanical Engineering, National Technical University of Athens, Zografou, 15772 Athens, Greece

[2] Faculty of Mechanical Engineering, University of Niš, 18000 Niš, Serbia

[3] Department of Mechanical Engineering, School of Engineering, University of West Attica, Egaleo, 250 Thivon & Petrou Ralli, 12244 Athens, Greece

[*]Corresponding author; E-mail: ctzivan@central.ntua.gr

In this work, a novel solar parabolic dish collector with an integrated rhombic Stirling engine is investigated. The collector is studied in steady-state conditions for several different operating cases, while an analytical solution is developed for calculating the useful power output as a function of the receiver's temperature. The results are successfully verified via a numerical model developed in SolidWorks software, resulting in deviations lower than 5.3%. Subsequently, the verified analytical solution is used for conducting a parametric study in which the aperture diameter of the dish is modified, considering a receiver temperature range from 300 to 600ºC. The collector's thermal efficiency is calculated for each operating case. Moreover, the mechanical efficiency of the Stirling engine is calculated via a developed model. The overall efficiency is then calculated, and the optimum operating point in each diameter case is revealed. The maximum overall efficiency considering a reflector's outer diameter of 1.2 m is calculated at 38.71%, whereas it is determined at 41.51% for a diameter of 1.4 m. Finally, it is found that the greater the diameter, the higher the optimum efficiency and the receiver temperature at which the optimum efficiency is achieved.

Key words: *Solar Collector, Parabolic Dish Concentrator, Stirling Engine, Numerical model, Analytical solution*

1. Introduction

In the last decades, the energy problem has been one of the most critical issues that humanity faces. The rapidly advancing technology combined with the increase in world population is leading to an increased energy demand, which humanity is called to cover via energy production technologies [1]. In previous years, humanity's growth was strongly dependent on fossil fuels such as carbon, oil, and natural gas. However, these sources of energy are not limitless, and thus, new energy sources and technologies to exploit them must be investigated to secure the continuous technological advancement and human growth [2]. Renewable energy sources consist of a reliable and sustainable solution for this

problem, as well as addressing air pollution and climate change [3]. Among the renewable energies, solar irradiation seems to be the most promising option.

In the literature, a lot of research has been conducted considering Concentrated Solar Power (CSP) as one of the most effective ways to utilize solar irradiation for power and heat production [4]. CSP technologies can be mainly classified, based on the type of their receiver, as linear or point focal technologies. The most representative technologies with linear receivers are the parabolic trough collector and the linear Fresnel collector [5]. Notably, many studies focus on concentrating solar collectors. More specifically, Korres and Tzivanidis [6] examined an evacuated double cavity receiver parabolic trough collector and compared it with an ordinary geometry. Korres et al. [7] investigated a twin cavity receiver coupled with a parabolic trough collector. In addition, Ahmadpour et al. [8] modeled a linear Fresnel reflector solar concentrator using a Monte Carlo ray tracing method. The most representative point focal receiver technologies are the solar tower and the Parabolic Dish Collector (PDC) [5]. Indicatively, Atif and Al-Sulaiman [9] analyzed the energetic and exergetic performance of solar-driven supercritical CO_2 recompression cycles, where the solar tower was the examined CSP technology. The PDC technology is almost always integrated with a Stirling Engine (SE), placed at its focal point receiver. The SE cycle consists of two isothermal (constant-temperature) and two constant-volume processes. The high temperature of the Stirling cycle can be up to 1000°C [10], whereas the low temperature ranges from 30 to 50°C [11]. When coupled with PDC, one part of the SE is exposed to solar irradiation, whereas the other side includes external fins to cool the working fluid, which can be air [12]. The main types of SEs are alpha, beta, and gamma types [12]. Furthermore, SEs are separated into four types, i.e., free-piston, liquid piston, thermoacoustic, and kinetic [13]. In kinetic SEs, also known as crank-driven, the work is produced because of the movement of a slider-crank mechanism, following the expansion of the working medium due to the thermal input from the concentrated solar irradiation at the focal point of the receiver where the SE is located. The thermoacoustic SE replaces the slider-crank mechanism with an acoustic wave, whereas in the liquid piston SE, this mechanism is replaced by water columns. Free-piston SEs consist of a spring system rather than a slider-crank mechanism [13]. Research efforts have also been made on the integration of SE with other CSP technologies, besides the PDC. For instance, Zhu et al. [14] analyzed the integration of an SE with a parabolic trough collector for electricity production. Rabhi et al. [15] investigated a gamma-type SE also coupled with a linear Fresnel concentrating solar collector. Furthermore, many studies have been conducted with PDC coupled to SEs. Mehrpooya et al. [16] investigated the combination of a PDC, an SE, and a thermoelectric device, while the optimum overall efficiency was found to be 39.17%. Singh and Kumar [12] presented a review of the development and performance of solar SEs. Additionally, Lashari et al. [17] performed a techno-economic investigation of PDC combined with the SE, whereas Awan et al. [18] integrated this system with photovoltaics.

The present study examines the integration of a PDC system with a rhombic-driven SE of high efficiency. The SE is placed on the base of the parabola, minimizing the shading losses and maximizing the optical efficiency of the unit. The analytical solution calculates the useful power output for various operating points by varying the receiver's temperature. The mechanical efficiency is calculated based on an adiabatic analysis of a single-cylinder beta-type rhombic-driven SE, using Mathcad software, assuming that there is a highly efficient machine. The novelty of this investigation lies in the optimization of the solar dish design by incorporating different tools, a fact leads to the development of a highly efficient configuration. It is highlighted that the analytical solution is verified using the

SolidWorks Flow Simulation studio. For each operating point, a modification of the PDC diameter is conducted to detect the optimum diameter. It has been evidenced that an increase in the diameter leads to a rise in the optimum overall efficiency of the system, and the receiver's temperature at which this efficiency is achieved is higher.

2. Material and methods

2.1. The studied solar Stirling engine

The proposed solar SE is a beta-type rhombic-driven engine, and it exploits solar energy through a parabolic dish reflector. **Fig. 1** illustrates the system geometry examined. Solar rays are concentrated on the warm part of the engine as a result of the reflectance of the parabolic dish, heating it and allowing it to operate. It has to be mentioned that the illustrated system does not include the regenerator and the cooler of the SE, since these two parts are not simulated in the present work. As can be observed in **Fig. 1**, solar irradiation is focused on the peripheral surface of the SE's heater, while the heater is exposed to ambient conditions. A part of the parabolic dish reflector at its center has been trimmed for the SE to be integrated properly with the solar dish. It is important to mention that, in the most common integration of solar SEs with a dish reflector, the SE is located against the mirror, a fact that significantly reduces the utilized solar irradiation due to shading losses. This happens because PDC always tracks the sun's position using a two-axis tracking mechanism. So, if the SE is located on the focal point of the parabola, it is also located between the PDC and the sun, and, as a result, the SE shades a part of the available reflectance area. In the proposed collector, the SE is located on the base of the reflector to ensure the maximum possible exploitation of the available solar energy, avoiding a significant amount of shade losses. The dimensions of the SE are presented in **Tab. 1**. Specifically, the aperture area of the collector is 1.13 m^2, the outer diameter of the dish is 1.2 m, the inner diameter of the dish is 0.08 m, the focal distance is 0.195 m, the Stirling Engine outer diameter is 0.03 m and the heater length is 0.2 m.

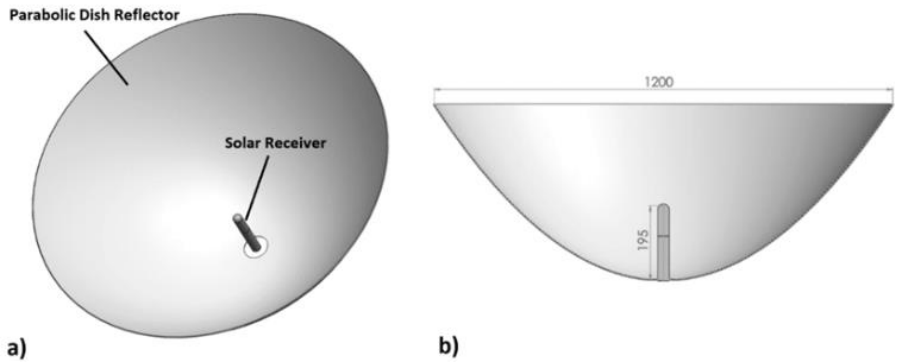

Figure 1. Geometry of the solar Stirling engine: a) 3D view and b) main dimensions.

Table 1. Solar Stirling Engine and dish dimensions.

Parameter	Symbol	Value	Units
Aperture area	A_a	1.13	m^2
Outer dish diameter	D_{out}	1.20	M
Inner dish diameter	D_{in}	0.08	M
Focal length	L_F	0.195	M
Stirling Engine outer diameter	$D_{SE,out}$	0.03	M
Heater length	L_h	0.20	M

2.2. Mathematical formulation

The main mathematical formulas used in this analysis are presented in this section. The radiative thermal losses ($Q_{L,rad}$) of the collector are given by eq. (1) where the temperature (T) is in Kelvin units, with the respective convective losses ($Q_{L,cnv}$) to follow in eq. (2).

$$Q_{L,rad} = A_r \cdot \varepsilon_r \cdot \sigma \cdot ({T_r}^4 - {T_{amb}}^4) \quad (1)$$

$$Q_{L,cnv} = A_r \cdot h_w \cdot (T_r - T_{amb}) \quad (2)$$

The total thermal losses ($Q_{L,tot}$) are the summation of the radiative and the convective thermal losses as eq. (3) suggests. The useful power (Q_u) can then be calculated from eq. (4) by subtracting the overall thermal losses from the absorbed solar power.

$$Q_{L,tot} = Q_{L,rad} + Q_{L,cnv} \quad (3)$$

$$Q_u = Q_{abs} - Q_{L,tot} \quad (4)$$

The absorbed solar power (Q_{abs}) is calculated via eq. (5) considering the reflectance of the dish concentrator (ρ), the absorptance of the receiver (α), and the available solar power (Q_s) on the aperture of the collector. The last one is calculated through eq. (6) having as an input the solar beam irradiation intensity perpendicular to the aperture area of the dish (G_T) and the total aperture (A_a).

$$Q_{abs} = \alpha \cdot \rho \cdot Q_s \quad (5)$$

$$Q_s = A_a \cdot G_T \quad (6)$$

The thermal efficiency (η_{th}) expression is given by eq. (7) as the quotient of the useful product to the available solar irradiation on the aperture.

$$\eta_{th} = \frac{Q_u}{Q_s} \quad (7)$$

The electrical efficiency (η_{el}) can be calculated using eq. (8) as the quotient between the electrical output (P_{el}) and the useful power (Q_u). Also, the electrical efficiency can be defined as the product of the mechanical efficiency (η_{mech}) and the electromechanical conversion efficiency (η_{elmc}). Finally, the overall performance ($\eta_{overall}$) is calculated via eq. (9) considering the thermal and electrical efficiencies.

$$\eta_{el} = \eta_{mech} \cdot \eta_{elmc} = \frac{P_{el}}{Q_u} \quad (8)$$

$$\eta_{overall} = \eta_{th} \cdot \eta_{el} \quad (9)$$

2.3. Methodology

2.3.1 Analytical model

The analytical solution developed in this study is presented in this section in detail. It is worth mentioning that the main parameter that varies is the receiver temperature, while thermal efficiency and useful power are the main outputs in each calculation. It is significant to state that overall efficiency is the most important index for the evaluation of the system's performance since it determines the optimum operating point of the system. To begin with, a value for the receiver temperature is initially considered. Then, the radiation and the convective losses of the collector are calculated using eq. (1) and eq. (2), considering a constant wind heat transfer coefficient and a constant ambient temperature. The summation of the pre-mentioned losses through eq. (3) results in the overall thermal losses of the collector. Afterward, the useful power is calculated by subtracting the calculated losses from the absorbed solar power according to eq. (4). It is important to state that, for the analytical calculations, the absorbed solar power is calculated by the product of the available solar power on the aperture, the absorptance of the receiver, and the reflectance of the dish mirror as in eq. (5) indicates. The available solar power is then calculated via eq. (6) and finally, the thermal efficiency is found by eq. (7) and the electrical efficiency based on eq. (8). Finally, the overall efficiency of the unit is found using eq. (9).

2.3.2 Simulation model

To verify the analytical approach, a numerical model is developed in the SolidWorks Flow Simulation studio [19]. This simulation package has also been applied in a wide range of applications related to solar energy utilization, and it has been proven to be a reliable and valid tool [20, 21]. There is a wide portfolio in the international scientific literature in which studies with SolidWorks in the field of solar energy can be found, and most importantly, a significant number of studies where the simulation results are validated using real experimental data [22, 23] and verification with various analytical approaches [20, 51]. In this study, a numerical model is developed considering the same operating conditions as in the analytical approach. The collector is designed in SolidWorks, and the necessary boundary conditions are applied in the model. The proper absorptance and reflectance coefficients are defined on the receiver's and the reflector's surfaces, respectively, through the related libraries of the simulation tool. Both the wind heat transfer coefficient and the ambient air temperature are set on the surface of the receiver as boundary conditions via the "Boundary Conditions" selection, to simulate the convective regime between the receiver surface and the ambient air. The solar energy that falls perpendicular to the aperture of the collector, the sky temperature, and the analysis type are all set on the "Analysis Type" tab. It is significant to mention that the sky temperature is the same as the ambient temperature since the receiver's surface is mostly facing the reflector rather than the sky, and also because the reflector's temperature is near the ambient air one. The analysis is conducted on steady-state conditions. An important input is the useful power as calculated by the analytical solution. In particular, the analytically calculated useful power for each receiver temperature is set as an input in the simulation model with a negative sign, for the heater of the SE to be the heat sink for the simulation. Thus, a useful power is set with a negative sign on the inner surface of the receiver, and the respective temperature is calculated by the simulation. Practically, the scope of the simulation is to verify how close the simulation values for the receiver temperature are to the respective analytical values, considering the same thermal efficiency in each solution (numerical, analytical). Receiver temperatures resulting from the simulations are expected to be different than the analytical ones, considering the same useful power and thus each thermal efficiency value is achieved for different receiver temperature which means that different operating points are expected for considering the same heat sink in both the analytical and the numerical solution. For a reliable interpretation of the comparative results, the thermal efficiency curves of both solutions were compared.

2.3.3 Sensitivity analysis

A sensitivity analysis is conducted to guarantee the reliability of the applied numerical model. More specifically, the main goal is the independence of the absorbed solar energy from the grid. Thus, a mesh independence analysis is carried out considering several different meshes, assuming that the convergence criterion is the absorbed solar power value. Rigorous focus is given to the mesh grid structure regarding the surfaces that receive solar irradiation, with several refinements to be applied. In particular, in the first stage of the independence analysis, three different receiver surface local meshes are tested, considering the global mesh as constant, and the optimum mesh is finally selected. The selected mesh is further processed considering the local mesh structure pattern on the receiver as constant, and the global mesh to be modified. The optimum mesh is finally selected and applied in simulation studies. It is important to state that the number of simulated rays is set to 10^7 to ensure a reliable ray tracing analysis independent of the solar rays. **Tab. 2** and **Tab. 3** present the meshes that are

evaluated in each of the two stages of the independence analysis, with RLM standing for the Receiver's Local Mesh. Finally, an RLM level of three and $4.21 \cdot 10^5$ elements are used.

Table 2. Results of the sensitivity analysis (Stage 1).

Mesh name	A_1	B_1	C_1
RLM refinement level	2	3	4
Global mesh dimensions (X-Y-Z)	50-25-50	50-25-50	50-25-50
Elements ($\times 10^5$)	1.04	1.08	1.21
Q_{abs} (W)	967	974	975

Table 3. Results of the sensitivity analysis (Stage 2).

Mesh name	A_2 (B_1)	B_2	C_2	D_2	E_2
RLM refinement level	3	3	3	3	3
Global mesh dimensions (X-Y-Z)	50-25-50	60-30-60	70-35-70	80-40-80	100-50-100
Elements ($\times 10^5$)	1.08	1.72	2.95	4.21	6.91
Q_{abs} (W)	974	988	991	993	994

2.3.4 Properties and operating conditions

The proposed system is examined considering several different operating conditions, mainly regarding the receiver's temperature. The most important operating conditions are presented in **Tab. 4**. The environmental temperature, the heat transfer coefficient, and the solar irradiation perpendicular to the aperture are supposed to be steady. The main optical properties regarding the reflectance and the absorptance of the reflector and the absorptive surface respectively, as well as the parameters regarding the thermal radiation exchange, are presented in **Tab. 5**. It is significant to mention that the values for the absorptance and the emittance of the receiver are set according to Ref. [25] for a receiver temperature of 700°C, considering that the optical and thermal properties of the coatings decline with the temperature increase and that in the present study, the examined receiver temperatures are lower than 700°C. Moreover, the selected mirror reflectance value is a typical one, and it appears in numerous other similar studies in the literature [16].

Table 4. Boundary conditions for simulation analysis.

Parameter	**Symbol**	**Value**	**Unit**
Solar irradiation	G_T	1000	W m^{-2}
Ambient temperature	T_{amb}	25	°C
Ambient heat transfer coefficient	h_w	10	W m^{-2} K^{-1}
Receiver temperature	T_r	300-600	°C

Table 5. Optical and thermal properties of the materials.

Parameter	**Symbol**	**Value**	**Unit**
Absorptance of the receiver	α	0.94	-
Reflectance of the concentrator	ρ	0.94	-
Emittance of the receiver	ε_r	0.373	-
Constant of Stefan-Boltzmann	σ	5.67×10^{-8}	W m^{-2} K^{-4}

2.3.5 Geometrical optimization

The system examined is optimized regarding the overall efficiency maximization. This analysis is based on the modification of the collector's aperture and specifically of the dish's outer diameter. Several different values are considered regarding the reflector's outer diameter (D_{out}) from 0.8 m up to 2.0 m with an interval step of 0.2 m. The thermal and electrical efficiency are calculated for each examined diameter, and thus the overall efficiency is revealed. The maximum value of the overall performance determines the optimum operating point for each examined case. The effect of the variation of the outer reflector's diameter is also taken into consideration to determine the optimum value among

the optimum overall efficiencies. Thus, the diameter case in which the maximization of the overall efficiency is achieved is finally selected.

2.3.6 Rhombic-driven Stirling engine analysis

The examined engine is a single-cylinder beta-type rhombic-driven SE, of which modeling is based on the GPU-3 model of General Motors [26]. **Tab. 6** presents the SE's specifications and characteristics. The thermodynamic analysis is adiabatic, neglecting all kinds of losses and this model tries to simulate an optimistic scenario with a highly efficient engine. The selected working fluid is Helium, a common selection that also appears in other studies in the literature [27]. The model of this beta-type rhombic-driven SE is developed in Mathcad, a useful software for model analysis and calculations [28]. First, SE's pressure and temperature at its different stages are initialized. These stages are the heater, the cooler, and the regenerator. The boundary conditions of the temperatures on the interfaces between the compressor and cooler, cooler and regenerator, and finally, heater and expander are set, as presented in **Tab. 6**. The value of the heater temperature is assigned as initialization to the expander, and the interface between the expander and the heater, whereas the value of the cooler temperature is assigned to the compressor and the interface between the compressor and the cooler.

Table 6. Stirling Engine's specifications and operational parameters.

Parameter	Symbol	Value	Unit
Number of cylinders	N	1	-
Crank radius	r_{cra}	$1.38 \cdot 10^{-2}$	m
Piston bore	D_{pb}	$2.96 \cdot 10^{-2}$	m
Expansion clearance volume	V_{cle}	30.52	cm^3
Compression clearance volume	V_{clc}	29.68	cm^3
Heater temperature	T_h	300-400	°C
Cooler temperature	T_{co}	15	°C
Frequency	f	41.72	Hz

The pressure change (P) is calculated through eq. (10) as a function of the crank angle (θ), the temperature (T_i), the working medium specifications, and the volumes (V_i) of the different SE sections, with the volume in cubic meters rather than cubic centimeters. The temperature of the regenerator (T_{reg}) is calculated through eq. (11).

$$P(\theta) = \frac{M \cdot R}{\frac{V_c(\theta)}{T_{co}} + \frac{V_e(\theta)}{T_h} + \frac{V_{co}}{T_{co}} + \frac{V_{reg}}{T_{reg}} + \frac{V_h}{T_h}} \tag{10}$$

$$T_{reg} = \frac{T_h - T_{co}}{ln\left(\frac{T_h}{T_{co}}\right)} \tag{11}$$

Tab. 7 presents the volumetric values of the SE. The temperature, total work, and heat flux of SE's stages are then defined, allowing the final determination of the system's mechanical efficiency. As far as electromechanical conversion efficiency is concerned, a typical value of 98% is considered for the calculation of electrical power output. The mechanical efficiency of the engine is given in **Fig. 2** as a datum for the rest of the calculations planned to be conducted.

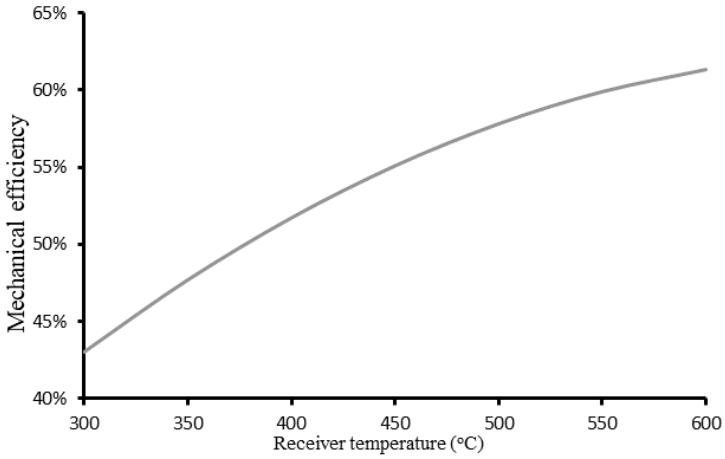

Figure 2. Mechanical efficiency of the Stirling Engine for different receiver temperatures.

Table 7. SE's characteristic volumes.

Parameter	Symbol	Value	Unit
Cooler's volume	V_{co}	$13.18 \cdot 10^{-6}$	m^3
Regenerator's volume	V_{reg}	$50.55 \cdot 10^{-6}$	m^3
Heater's volume	V_h	$70.28 \cdot 10^{-6}$	m^3

3. Results and discussion

3.1. Verification of the Analytical Approach

This section presents the comparison between the analytical and the numerical results. **Fig. 3** illustrates the thermal efficiency values for different receiver temperature levels as determined by the simulation tool and the analytical solution for the case of D_{out} equal to 1.2 m. As can be observed in **Fig. 3**, there is a sufficient agreement between the numerical and the analytical results, with deviations lower than 5.3%. The mean deviation is found to be 2.0% and hence, the verification of the analytical model is successfully achieved. Generally, in both methods, the thermal efficiency seems to decline with the increase of the receiver temperature, which is a reasonable fact due to the thermal losses increase.

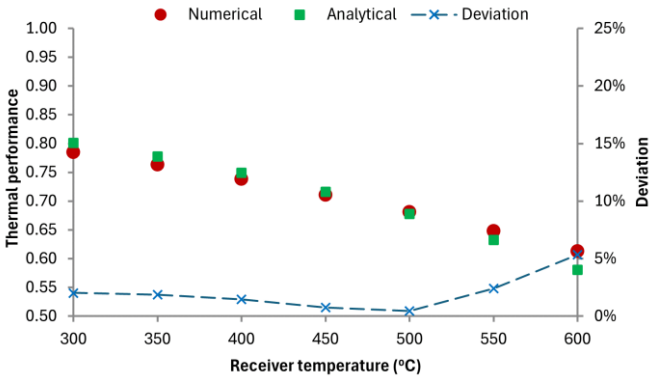

Figure 3. Verification of the analytical results for D_{out}=1.2 m for different receiver temperatures.

3.2. Overall analysis

3.2.1 Overall performance optimization for the initial geometry

Fig. 4 presents the thermal, electrical, and overall efficiency of the examined solar SE as a function of the receiver's temperature. According to **Fig. 4**, the thermal efficiency declines with the increase of the receiver temperature, while the electrical efficiency increases. It is important to say that the overall efficiency curve appears to have a total maximum value of around 460°C.

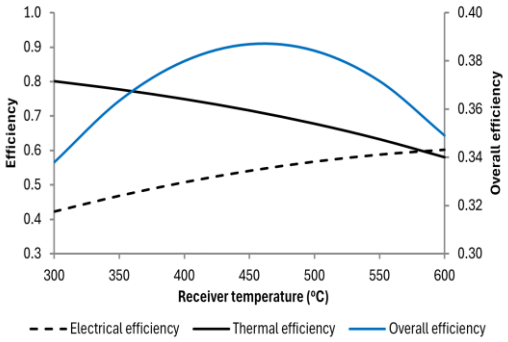

Figure 4. Thermal, electrical, and overall performance for D_{out}=1.2 m for different receiver temperatures.

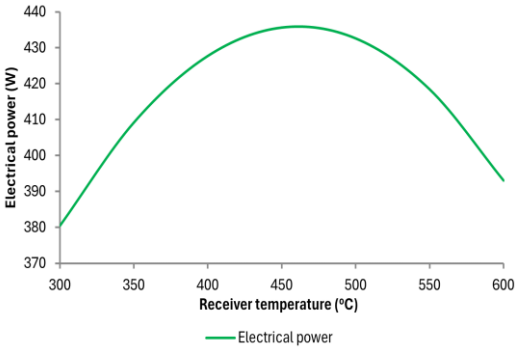

Figure 5. Electrical power for D_{out}=1.2 m for different receiver temperatures.

According to **Fig. 5**, the electrical power output is maximized at a particular receiver temperature level. Hence, this operating point represents the optimum electrical power for the case of using a reflector outer diameter of 1.2 m. The initial geometry (D_{out}=1.2 m) is analyzed both thermally and electrically for the receiver temperature range presented in **Tab. 4**.

3.2.2 Geometrical Optimization Results

This section presents the geometrical optimization results. **Fig. 6** depicts the overall performance for seven different outer diameters of the dish reflector as a function of the receiver temperature. It is interesting to note from **Fig. 6** that there is a maximization of the overall efficiency at a specific receiver temperature for each examined diameter, and this indicates that there is an optimum operating point in each case. This occurs mainly due to the rapid increase in thermal losses when the receiver temperature increases. Moreover, it is underlined that this overall efficiency maximization follows a different pattern in each case. When the diameter takes higher values, the optimum receiver temperature is also increased. For instance, the optimum receiver temperature for D_{out}=1.2 m is equal to 460°C while for D_{out}=1.4 m it is equal to 500°C. In addition, it can be observed that the increase of the outer reflector diameter leads to greater overall performance levels for all the operating points. For example, the maximum overall efficiency for D_{out}=1.2 m is found at 38.71% in contrast to 41.51% for D_{out}=1.4 m. However, the rate of this overall increase seems to decline, and the results seem to converge and become less dependent on the diameter of the reflector when having greater diameter values. This can be explained if a single receiver temperature is considered. In this case, the electrical efficiency is constant. Hence, thermal efficiency is the one to blame for the observed convergence and it is of great interest to investigate the reason why this occurs. For that reason, it would be a great choice to break the thermal efficiency into two quotients. The first one is the quotient between the absorbed solar energy and the available solar power, while the second one is between the heat losses and the available solar power.

The thermal efficiency is found by subtracting the second quotient from the first one. The first quotient remains constant for a specific receiver temperature. Thus, the quotient between thermal losses and the available solar energy affects the observed convergence. In particular, the thermal losses are constant considering a specific receiver temperature, while the available solar power fluctuates with the outer reflector diameter. Hence, the available solar power is the parameter that causes the observed convergence. **Fig. 7** shows the thermal efficiency and the two pre-mentioned quotients for a receiver temperature of 300°C, to clarify the convergence phenomenon observed in **Fig. 6**.

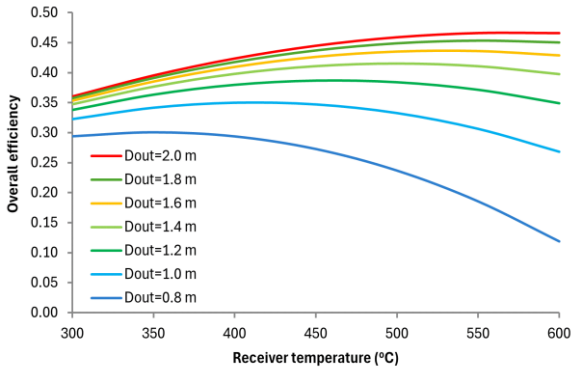

Figure 6. Overall performance for different outer reflector diameter values and for different receiver temperatures.

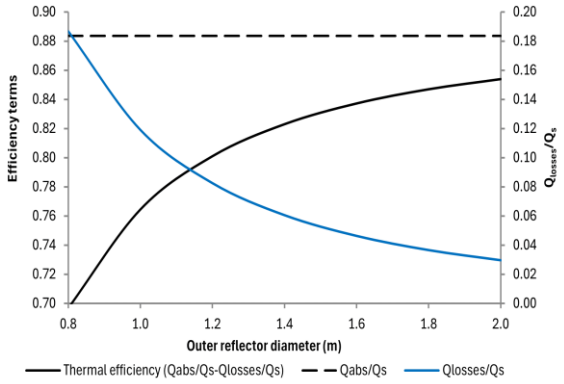

Figure 7. Detailed analysis of the thermal efficiency as a function of the outer reflector diameter for T_r=300°C.

The optimum receiver temperature and the maximum overall efficiency for different values of the outer reflector diameter and absorbed solar power are shown in **Fig. 8** and **Fig. 9**, respectively. **Fig. 8** depicts the optimum operating points for all the examined outer reflector diameter values. According to **Fig. 8**, it becomes obvious once again that the rate of the maximum overall efficiency increase reduces when the outer reflector diameter increases. The same behavior appears, also, in the optimum receiver temperature curve. This happens for the same reason as depicted in **Fig. 9,** with the additional factor that electrical efficiency also declines with the increase of the outer reflector diameter. Generally, regarding this specific analysis, it can be stated that the increase of the outer reflector diameter leads to greater overall performance at a decreasing rate. According to the results (**Fig. 8**), it seems that diameter values greater than 1.6 m do not contribute significantly to the overall performance enhancement. The optimal receiver temperature ranges from 350 to 560ºC, approximately, for different outer reflector diameters. Respective values are reported for the different absorbed solar power values.

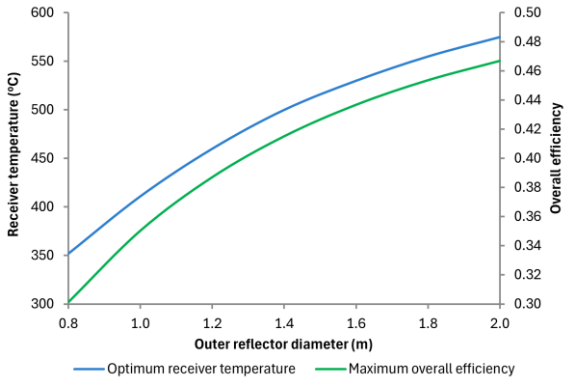

Figure 8. Optimum receiver temperature and maximum overall efficiency for various outer reflector diameter values.

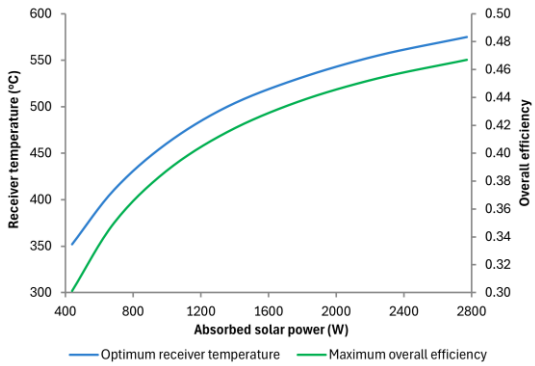

Figure 9. Optimum receiver temperature and maximum overall efficiency for various absorbed solar power values.

4. Conclusions

In this work, a solar rhombic-driven Stirling Engine with a parabolic dish reflector is investigated in detail. Generally, it is important to state that the suggested geometrical optimization seems to provide meaningful insights into the temperature range in which the Stirling engine operates more efficiently. Simultaneously, it reveals a wide range of possible combinations with reflectors, offering an overall

estimation regarding the selection of the proper combination based on the temperature and space limitations that may exist in related applications. The most significant outcomes are listed below:

- The numerical model for the thermal efficiency determination is verified by an analytical one, and the calculated deviations did not exceed 5.3%.
- The maximum overall efficiency for a reflector's diameter of 1.2 m is determined to be 38.71%, whereas for a reflector's diameter of 1.4 m is found to be 41.51%. Also, a greater reflector's diameter results in a higher overall efficiency of the system.
- The optimum receiver temperature for a reflector's diameter of 1.2 m is equal to 460°C, whereas for a reflector's diameter of 1.4 m it is equal to 500°C.
- There is a convergence in the overall efficiency increase when the reflector's diameter increases due to the greater availability of solar power.
- The increase in the receiver temperature does not ensure the rise of overall efficiency since there is a total maximum value of the overall efficiency in each reflector's diameter case. In other words, the overall efficiency declines after passing a specific operating temperature. This temperature limit is greater as the reflector diameter increases.

In the future, it would be very interesting to apply multi-objective optimization techniques for optimizing both the system energy efficiency and the economic sustainability. Moreover, the daily performance of the systems during the year for different climate conditions is another interesting option for further investigation.

Acknowledgments

Saša R. Pavlovic would like to thank the Serbian Ministry of Science, Technological Development and Innovation for the funding of project no. 451-03-47/2023-01/200156 "Innovative scientific and artistic research from the FTS (activity) domain".

Nomenclature

Variables		*Subscripts*	
A	Surface Area [m^2]	a	Aperture
D	Diameter [m]	abs	Absorbed
f	Frequency [Hz]	amb	Ambient
G	Solar Irradiation [W m^{-2}]	c	Compressor
h	Heat Convection Coefficient [W m^{-2} K^{-1}]	clc	Compression clearance
L	Length [m]	cle	Expansion clearance
M	Molecular weight [kg $kmol^{-1}$]	cnv	Convection
N	Number of cylinders	co	Cooler
P	Pressure [Pa]	cra	Crank
P_{el}	Electricity [W]	e	Expander
Q	Energy rate [W]	el	Electrical
R	Individual Gas Constant [kJ kg^{-1} K^{-1}]	elmc	Electromechanical
r	Radius [m]	F	Focal
T	Temperature [°C or K]	h	heater
V	Volume [cm^3 or m^3]	in	Inner
		L	Losses
Greek symbols		mech	Mechanical
α	Absorbance	out	Outer
ε	Emissivity	overall	Overall
η	Efficiency	pb	Piston bore
θ	Crank angle [°]	r	Receiver
ρ	Reflectance	rad	Radiative
σ	Stefan-Boltzmann constant [=5.67x10^{-8} W m^{-2} K^{-4}]	reg	Regenerator
		s	Solar

Abbreviations		T	Perpendicular to aperture
CSP	Concentrated Solar Power	th	Thermal
PDC	Parabolic Dich Collector	tot	Total
RLM	Receiver Local Mesh	u	Useful
SE	Stirling Engine	w	Wind

References

[1] Kannan, N., Vakeesan, D., Solar energy for future world: - A review, Renew. Sustain. Energy Rev., vol. 62, pp. 1092–1105, Sep. 2016, doi: 10.1016/j.rser.2016.05.022.

[2] T. S. Ge et al., Solar heating and cooling: Present and future development, Renew. Energy, vol. 126, pp. 1126–1140, Oct. 2018, doi: 10.1016/j.renene.2017.06.081.

[3] Al-Shetwi, A. Q., Hannan, M. A., Jern, K. P., Mansur, M. T., Mahlia, M. I., Grid-connected renewable energy sources: Review of the recent integration requirements and control methods, J. Clean. Prod., vol. 253, p. 119831, Apr. 2020, doi: 10.1016/j.jclepro.2019.119831.

[4] Islam, M. T., Huda, N., Abdullah, A. B., Saidur, R., A comprehensive review of state-of-the-art concentrating solar power (CSP) technologies: Current status and research trends, Renew. Sustain. Energy Rev., vol. 91, pp. 987–1018, Aug. 2018, doi: 10.1016/j.rser.2018.04.097.

[5] Bellos, E., A geospatial comparative analysis of solar thermal concentrating power systems in Greece, Clean. Energy Syst., vol. 4, p. 100055, Apr. 2023, doi: 10.1016/j.cles.2023.100055.

[6] Korres, D. N., Tzivanidis, C., An innovative small-sized double cavity PTC under investigation and comparison with a conventional PTC, Sustain. Energy Technol. Assess., vol. 53, p. 102462, Oct. 2022, doi: 10.1016/j.seta.2022.102462.

[7] Korres, D. N., et al., An Innovative Parabolic Trough Collector Design with a Twin-Cavity Receiver, Appl. Sci., vol. 12, no. 24, p. 12551, Dec. 2022, doi: 10.3390/app122412551.

[8] Ahmadpour, A., et al., Optimization and modelling of linear Fresnel reflector solar concentrator using various methods based on Monte Carlo Ray–Trace, Sol. Energy, vol. 245, pp. 67–79, Oct. 2022, doi: 10.1016/j.solener.2022.09.006.

[9] Maimoon, Atif, Al-Sulaiman, F. A., Energy and exergy analyses of solar tower power plant driven supercritical carbon dioxide recompression cycles for six different locations, Renew. Sustain. Energy Rev., vol. 68, pp. 153–167, Feb. 2017, doi: 10.1016/j.rser.2016.09.122.

[10]Çınar, C., Aksoy, F., Solmaz H., Yılmaz E., Uyumaz, A., Manufacturing and testing of an α-type Stirling engine, Appl. Therm. Eng., vol. 130, pp. 1373–1379, Feb. 2018, doi: 10.1016/j.applthermaleng.2017.11.132.

[11]Hooshang, M., Moghadam, A., R. S., Nia, A., Masouleh, M. T., Optimization of Stirling engine design parameters using neural networks, Renew. Energy, vol. 74, pp. 855–866, Feb. 2015, doi: 10.1016/j.renene.2014.09.012.

[12]Singh, U. R., Kumar, A., Review on solar Stirling engine: Development and performance, Therm. Sci. Eng. Prog., vol. 8, pp. 244–256, Dec. 2018, doi: 10.1016/j.tsep.2018.08.016.

[13]Wang, K. S., Sanders, R. S., Dubey, F. H. Choo, Duan, F., Stirling cycle engines for recovering low and moderate temperature heat: A review, Renew. Sustain. Energy Rev., vol. 62, pp. 89–108, Sep. 2016, doi: 10.1016/j.rser.2016.04.031.

[14]Zhu, S., et al., A free-piston Stirling generator integrated with a parabolic trough collector for thermal-to-electric conversion of solar energy, Appl. Energy, vol. 242, pp. 1248–1258, May 2019, doi: 10.1016/j.apenergy.2019.03.169.

[15]Rabhi, L., Khmou, A., Boutammachte, N., Parametric investigation on a Gamma type Stirling engine efficiency coupled to Linear Fresnel Solar Collector, 1st International Conference on Innovative Research in Applied Science, Engineering and Technology (IRASET), Meknes, Morocco: IEEE, Apr. 2020, pp. 1–4. doi: 10.1109/IRASET48871.2020.9092029.

[16]Mehrpooya, M., Ghadimi, N., Marefati, M., Ghorbanian, S. A., Numerical investigation of a new combined energy system includes parabolic dish solar collector, Stirling engine and thermoelectric device, Int. J. Energy Res., vol. 45, no. 11, pp. 16436–16455, Sep. 2021, doi: 10.1002/er.6891.

[17]Lashari, A. A., Shaikh, P. H., Leghari, Z. H., Soomro, M. I., Memon, Z. A., Uqaili, M. A., The performance prediction and techno-economic analyses of a stand-alone parabolic solar dish/stirling system, for Jamshoro, Pakistan, Clean. Eng. Technol., vol. 2, p. 100064, Jun. 2021, doi: 10.1016/j.clet.2021.100064.

[18]Awan, A. B., Zubair, M. Z., Memon, A., Ghalleb, N., Tlili, I., Comparative analysis of dish Stirling engine and photovoltaic technologies: Energy and economic perspective, Sustain. Energy Technol. Assess., vol. 44, p. 101028, Apr. 2021, doi: 10.1016/j.seta.2021.101028.

[19]Matsson, J., An Introduction to SOLIDWORKS Flow Simulation 2015. [Online]. Available: https://static.sdcpublications.com/pdfsample/978-1-58503-934-0-2.pdf

[20]Bellos, E., Tzivanidis, C., Antonopoulos, K. A., Gkinis, G., Thermal enhancement of solar parabolic trough collectors by using nanofluids and converging-diverging absorber tube, Renew. Energy, vol. 94, pp. 213–222, Aug. 2016, doi: 10.1016/j.renene.2016.03.062.

[21]Korres, D., Tzivanidis, C., A new mini-CPC with a U-type evacuated tube under thermal and optical investigation, Renew. Energy, vol. 128, pp. 529–540, Dec. 2018, doi: 10.1016/j.renene.2017.06.054.

[22]Korres, D. N., Tzivanidis, C., Koronaki, I. P., Nitsas, M. T., Experimental, numerical and analytical investigation of a U-type evacuated tube collectors' array, Renew. Energy, vol. 135, pp. 218–231, May 2019, doi: 10.1016/j.renene.2018.12.003.

[23]Korres, D. N., Tzivanidis, C., A novel asymmetric compound parabolic collector under experimental and numerical investigation," Renew. Energy, vol. 199, pp. 1580–1592, Nov. 2022, doi: 10.1016/j.renene.2022.08.030.

[24]Korres, D. N., Bellos, E., Tzivanidis, C., Integration of a Linear Cavity Receiver in an Asymmetric Compound Parabolic Collector, Energies, vol. 15, no. 22, p. 8635, Nov. 2022, doi: 10.3390/en15228635.

[25]Wang, H., Haechler, I., Kaur, S., Freedman, J., Prasher, R., Spectrally selective solar absorber stable up to 900 °C for 120 h under ambient conditions, Sol. Energy, vol. 174, pp. 305–311, Nov. 2018, doi: 10.1016/j.solener.2018.09.009.

[26]Urieli, I., Berchowitz, D. M., Stirling cycle engine analysis. in Modern energy studies. Bristol: A. Hilger, 1984.

[27]Yang, H.-S., Cheng, C.-H., Huang, S.-T., A complete model for dynamic simulation of a 1-kW class beta-type Stirling engine with rhombic-drive mechanism, Energy, vol. 161, pp. 892–906, Oct. 2018, doi: 10.1016/j.energy.2018.07.159.

[28]"Mathsoft Mathcad11 - User's Guide."

Paper submitted: July 7, 2025

Paper revised: August 5, 2025

Paper accepted: August 6, 2025